

Magnetoplasmon excitations in an array of periodically modulated quantum wires

B. P. van Zyl

*Institute for Microstructural Sciences, National Research Council of Canada, Ottawa, Ontario,
K1A 0R6*

E. Zaremba

Department of Physics, Queen's University, Kingston, Ontario, Canada K7L 3N6

Abstract

Motivated by the recent experiment of Hochgräfe *et al.*, we have investigated the magnetoplasmon excitations in a periodic array of quantum wires with a periodic modulation along the wire direction. The equilibrium and dynamic properties of the system are treated self-consistently within the Thomas-Fermi-Dirac-von Weizsäcker approximation. A calculation of the dynamical response of the system to a far-infrared radiation field reveals a resonant anticrossing between the Kohn mode and a finite-wavevector longitudinal excitation which is induced by the density modulation along the wires. Our theoretical calculations are found to be in excellent agreement with experiment.

73.20.Mf, 73.23.-b, 73.20.Dx

I. INTRODUCTION

Modern microstructuring techniques have made it possible to experimentally study a wide variety of low-dimensional electron systems such as quantum dots, wires and rings.¹ These systems are usually fabricated starting from a two-dimensional electron gas (2DEG) located at a modulation-doped semiconductor heterojunction. The application of laterally microstructured metallic gates² or the use of deep-mesa etching techniques³ allow for the precise patterning of the 2DEG. Over the past 15 years, a great deal of information has been obtained about the transport and far-infrared (FIR) optical properties of these systems. For example, magneto-transport measurements of laterally modulated 2DEG's reveal interesting magnetoresistance oscillations associated with the commensurability of the cyclotron radius and modulation period a .¹ Far-infrared transmission experiments, on the other hand, reveal a rich spectrum of collective excitations whose frequencies exhibit novel magnetic field dispersions.⁴

In this paper, we are interested in the magnetoplasmon excitations of an array of parallel quantum wires which are also periodically modulated along their length. Such a system was recently fabricated by Hochgräfe *et al.*,⁵ and studied using FIR transmission spectroscopy. They observe a pair of collective excitations which appear to interact and anticross as a function of magnetic field. This behaviour is qualitatively explained by elementary considerations of the magnetoplasmon mode spectrum of a uniform wire as described by the theory of Eliasson *et al.*⁶ The periodic modulation along the length of the wires acts as a grating-coupler which couples the Kohn mode to a finite-wavevector 1D magnetoplasmon of the uniform wire. The experimental data also show a novel kink-like feature in the vicinity of the cyclotron frequency ω_c , that was neither discussed, nor explained in Ref. [5].

Our purpose here is to theoretically investigate the system studied by Hochgräfe *et al.* in order to better understand the nature of the magnetoplasmon excitations observed. In particular, we would like to gain some insight into the nature of the periodic modulation of the electronic density in these systems, and how this leads to the coupling of the modes discussed above. To this end, we adopt a hydrodynamic theory based on the Thomas-Fermi-Dirac-von Weizsäcker (TFDW) approximation. This approach has already been used to describe the collective excitations in laterally modulated 2DEG's⁷ as well as other low-dimensional electronic structures.⁸⁻¹¹ Its main virtue is that it treats the ground state and dynamic properties of the system in a consistent fashion.¹² Our earlier successful applications give us confidence that the approach is able to accurately describe the collective excitations in the systems studied in Ref. [5].

The plan of the paper is as follows. In Sec. II we define our model for a periodically modulated quantum wire array. Then, we systematically analyze the effects of this modulation on the ground state, and dynamical properties of the system. To the extent possible, we make direct comparisons with the experiment of Ref. [5]. Finally, in Sec. III, we present our concluding remarks.

II. MODULATED WIRES

The TFDW approximation to the ground state of a quantum confined 2DEG is given by (atomic units are used throughout)^{7,10,11}

$$\begin{aligned}
E[n] = & \int d^2\mathbf{r} \left[\frac{\pi}{2}n^2 + \frac{\lambda_w}{8} \frac{|\nabla n(\mathbf{r})|^2}{n(\mathbf{r})} - \frac{4}{3} \sqrt{\frac{2}{\pi}} n^{3/2} \right] \\
& + \frac{1}{2} \int d^2\mathbf{r} \int d^2\mathbf{r}' \frac{n(\mathbf{r})n(\mathbf{r}')}{|\mathbf{r} - \mathbf{r}'|} + \int d^2\mathbf{r} v_{\text{ext}}(\mathbf{r})n(\mathbf{r}) .
\end{aligned} \tag{1}$$

The first term is the Thomas-Fermi approximation to the kinetic energy, the second term is a von Weizsäcker-like gradient correction, and the third term is the Dirac local exchange energy. For simplicity we neglect a correlation energy contribution which in any case has a small effect. The last two terms characterize the Hartree self-energy of the electrons and the interaction with the external potential, respectively. Once the confining potential $v_{\text{ext}}(\mathbf{r})$ has been defined, the variational minimum of Eq. (1) yields the ground state electronic density, $n_0(\mathbf{r})$, for the system of interest.^{7,10,11} To describe the array of modulated quantum wires in [5] we adopt a confining potential having the form¹³

$$v_{\text{ext}}(x, y) = \frac{1}{2}\omega_0^2 x^2 + V_y \cos(Gy) , \tag{2}$$

with $G = 2\pi/a$. It is understood that the potential in Eq. (2) is centered in each unit cell and periodically extended throughout the array with period a . Setting $V_y = 0$ describes a periodic array of parabolically confined quantum wires, whereas $V_y \neq 0$ provides a modulation along the wire direction, also with period a (see Fig. 1). Keeping in mind that the samples in [5] are prepared from a modulation-doped AlGaAs/GaAs heterostructure, the appropriate physical parameters are: the effective Bohr radius $a_0^* = 103 \text{ \AA}$ and the effective Rydberg of energy, $\text{Ry}^* = e^2/2\epsilon a_0^* = 5.4 \text{ meV}$. In these units, a 2D electronic density of $1.0 \times 10^{11} \text{ cm}^{-2}$ is given by $\bar{n}_{2D} = 0.10(a_0^*)^{-2}$, and an energy of $0.5 \text{ a.u.} = 1\text{Ry}^*$ is equivalent to 43.57 cm^{-1} .

In Fig. 1 we present the equilibrium density distributions for a small section of the array. Figure 1(a) is generated with the following physical parameters: an average density $\bar{n}_{2D} = 1.0 \times 10^{11} \text{ cm}^{-2}$, $a = 600 \text{ nm}$, $\omega_0 = 0.427 \text{ a.u.}$, and $V_y = 1 \text{ a.u.}$ As will be discussed in more detail later, this choice allows us to reproduce much of the experimental results⁵ obtained with the sample having a density of $\bar{n}_{2D} = 1.2 \times 10^{11} \text{ cm}^{-2} = 0.12(a_0^*)^{-2}$. We therefore believe that the very strongly modulated density shown is typical of the densities studied in the experiments. In Fig. 1(b), we show the effect of keeping the confining potential fixed and doubling the 2D density to $\bar{n}_{2D} = 0.2$. It can be seen that the degree of corrugation is reduced in both directions, and that the densities from adjacent wires are now beginning to overlap. In going from Fig. 1(b) to Fig. 1(c) we have doubled the strength of the modulation to $V_y = 2 \text{ a.u.}$ This gives rise to a much stronger modulation of the density along the length of the wires which now appear as a string of quantum dots. This is the density profile used to simulate the FIR response of the system as described in the second half of the experimental study in Ref. [5]. Finally, in Fig. 1(d), we show the density profile generated with the same potential parameters as in Fig. 1(c), but with a further 50% increase in the average density. This density takes on the character of an array of coupled quantum dots.

The dynamics of a mesoscopic system within the TFDW approach is governed by a set of (linearized) hydrodynamic equations,^{7,10,11}

$$\frac{\partial \delta n}{\partial t} + \nabla \cdot (n_0 \mathbf{v}) = 0 , \tag{3}$$

with $\delta n(\mathbf{r}, t) = n(\mathbf{r}, t) - n_0(\mathbf{r})$, and

$$\frac{\partial \mathbf{v}}{\partial t} = -\gamma \mathbf{v} - \nabla U^{\text{int}} + \mathbf{F}^{\text{ext}}. \quad (4)$$

Eq. (3) is the usual continuity equation, and Eq. (4) is a statement of Newton's second law. The quantity U^{int} plays the role of an effective potential for the internal force fluctuations, and \mathbf{F}^{ext} is the force due to any additional external electromagnetic fields imposed on the system, including a homogeneous, static magnetic field oriented normal to the 2DEG. In Eq. (4), we have also included a phenomenological viscous damping term, $-\gamma \mathbf{v}$, to account for Drude scattering. This term has the effect of giving the collective modes a finite lifetime.

The solution of Eqs. (3) and (4) allows us to calculate the physically relevant, time-averaged FIR power absorption.^{7,10,11,14} In terms of the induced current density $\mathbf{j}^{\text{ind}}(\mathbf{r}, t) = -n_0(\mathbf{r})\mathbf{v}(\mathbf{r}, t)$, we have

$$\langle P \rangle_t = \left\langle \int d^2 \mathbf{r} \, \mathbf{j}^{\text{ind}}(\mathbf{r}, t) \cdot \mathbf{E}^{\text{ext}}(\mathbf{r}, t) \right\rangle_t, \quad (5)$$

where

$$\mathbf{E}^{\text{ext}}(\mathbf{r}, t) = (E_x \hat{\mathbf{x}} + E_y \hat{\mathbf{y}}) \cos(\omega t) \quad (6)$$

is a spatially uniform radiation field polarized along ($E_x \neq 0$) or perpendicular to ($E_y \neq 0$) the direction of the wires. Most of our calculations are carried out for the perpendicular polarization, but some calculations are also done for the parallel polarization in order to identify some of the longitudinal excitations at low magnetic fields ($B \lesssim 0.5\text{T}$).

The theoretical FIR power absorption for the density profile corresponding to Fig. 1(a) is shown in Fig. 2.¹⁵ The curves are displayed in steps of $\Delta B = 0.25\text{T}$ starting at $B = 0\text{T}$, and are offset vertically for clarity. The dashed lines are guides to the eye and indicate the peak trajectories; the open symbols at the end of each line serve to label the different magnetoplasmon modes (see Fig. 3). The $B = 0\text{T}$ trace shows an isolated peak at $\omega \simeq 37 \text{ cm}^{-1}$ which is very close to the parabolic confinement frequency ω_0 . This is a clear signature of the center-of-mass Kohn mode (KM) predicted by the generalized Kohn theorem,¹⁶ and corresponds to a rigid oscillation of the equilibrium density perpendicular to the wires. With increasing magnetic field, this peak at first shifts slightly to higher frequencies, but around $B \simeq 0.8\text{T}$, this trend is reversed with the appearance of a small shoulder to the high frequency side of the peak. The shoulder evolves into a separate peak which gains in oscillator strength and shifts to higher frequencies along the dashed line ending with the unfilled diamond. Although difficult to resolve, there is also a weak peak labeled by the unfilled triangle.

The positions of the absorption peaks as a function of magnetic field are displayed in Fig. 3. The unfilled symbols used in this figure correspond to the labels used to track the peak trajectories in Fig. 2. For comparison, the filled squares are the raw experimental data taken from Ref. [5]. The dashed lines in Fig. 3 are the cyclotron frequency ω_c and $2\omega_c$. We will discuss the solid curves below. The splitting of the upper experimental mode between $B = 1.5\text{T}$ and 2.5T is attributed in [5] to the presence of the Bernstein mode at $\omega = 2\omega_c$.¹⁷⁻¹⁹ Apart from this detail, it is clear that the TFDW results provide a smooth interpolation through the experimental points, and overall are in excellent agreement with the data. In

particular, the size and position of the anticrossing between the two lowest-lying branches (open circles and open diamonds) is well reproduced.

In order to explain the details of the magnetic dispersions in Fig. 3, it will prove useful to first consider the simpler case of a 2DEG which is modulated in one direction (see Ref. [7] for details). These systems were generated by setting $\omega_0 = 0$ in Eq. (2) and taking the modulation to be in the x -direction, i.e., $V_y \rightarrow V_x$. An additional weak density modulation along the wires will induce a coupling between the $q_y = 0$ modes of the wire to modes with wavevector $q_y \equiv G = 2\pi/a$. It is therefore of interest to see how the $q_y = 2\pi/a$ mode frequencies evolve as a function of magnetic field. In Figs. 4(a)-(c), we present the magnetic dispersions of a uniaxially modulated 2DEG at fixed $q_y = 2\pi/a$. The excitation spectrum for the weakly modulated system ($V_x = 0.25$ a.u.) is shown in Fig. 4(a) and essentially exhibits the magnetoplasmon dispersion of a homogeneous 2DEG. The dense spectrum of modes starting from $\omega = 0$ at $B = 0$ T are a result of the broken translational invariance in the modulation direction, and eventually evolve into a series of edge magnetoplasmons (EMP's). In Fig. 4(b) we show the magneto-dispersion for the moderately modulated 2DEG having a modulation $V_x = 1.25$ a.u. For this strength of modulation, one of the magnetoplasmon branches starting from $\omega \simeq 36$ cm⁻¹ acquires a weak negative dispersion and exhibits an anticrossing-like behaviour with a mode which has the character of an EMP.²⁰ The mode dispersing upward from $\omega \simeq 45$ cm⁻¹ is associated with the KM and continues to increase in frequency with increasing magnetic field.²⁰ Finally, in Fig. 4(c) we show the spectrum of the $q_y = 2\pi/a$ modes for a modulation amplitude of $V_x = 1.5$ a.u. In this modulation regime, the 1DMP has a pronounced negative dispersion for $B \lesssim 2$ T, and the gap associated with the anticrossing between the $q_y = 2\pi/a$ 1DMP and EMP modes has decreased.

We are now in a better position to comment on the details of the magnetic dispersions in Fig. 3. Several solid curves are shown which correspond to the smooth wire limit. The solid curve which is lowest at $B = 0$ is the dispersion relation of the $q_y = 0$ center-of-mass KM, namely,^{7,21}

$$\omega^2(B) = \omega_0^2 + \omega_c^2, \quad (7)$$

with $\omega_0 = 37.2$ cm⁻¹. The next two solid curves are the magnetic dispersions of the two $q_y = 2\pi/a$ modes calculated by taking $V_y = 0$ and $\omega_0 = 37.2$ cm⁻¹ in Eq. (2) and are analogous to the pair of modes starting from $\omega \simeq 45$ cm⁻¹ in Fig. 4(c). We thus conclude that the two branches denoted by open triangles and diamonds in Fig. 3 are derived from the $q_y = 2\pi/a$ KM and the $q_y = 2\pi/a$ 1DMP of the uniform wire array as discussed above. However, in the present situation, the $q_y = 2\pi/a$ 1DMP is in fact coupled to the $q_y = 0$ KM by the periodic modulation along the wires, which results in the anticrossing behaviour seen in the vicinity of $B = 1$ T. For $B \lesssim 1$ T, the mode indicated by open circles has the character of the KM, while for $B \gtrsim 1$ T, the mode changes over into the $q_y = 2\pi/a$ 1D EMP. A similar change in character occurs for the open diamond branch, but in the opposite sense. This is precisely the interpretation of the experimental results given in Ref. [5]. The highest energy branch (open triangles) corresponding to the weak high energy resonance in Fig. 3 is clearly the $q_y = 2\pi/a$ mode belonging to the upward dispersing bulk mode (see e.g., Fig. 4(c)). Finally, we note that the track of the lowest mode in Fig. 3 shows a small 'kink' at $\omega = \omega_c$. As we shall see below, this kink becomes more prominent as the density of the system is increased. We defer further discussion of this feature until then.

We next consider the effect of increasing the electronic density. This is achieved experimentally by means of illumination, and in one particular run resulted in an approximate doubling of the average density. To simulate this situation, we considered a system having a density of $\bar{n}_{2D} = 0.2$ and the same confining potential used to generate the results in Fig. 3. The density distribution in this case is shown in Fig. 1(b) where it can be seen that the modulation of the density along the wires is weaker than for $\bar{n}_{2D} = 0.1$. However, the simple assumption of an increase in the electron density was not able to account for the observed trends in the experimental data. Indeed, agreement with experiment could only be achieved by simultaneously increasing the amplitude of the modulation potential to $V_y = 2$ a.u. The corresponding density distribution is shown in Fig. 1(c). The modulation of the density along the wires is clearly more pronounced than in Figs. 1(a) or 1(b). In Fig. 5, we present the calculated FIR power absorption. As in Fig. 2, there is a strong KM peak at $B = 0$ T, consistent with the parabolic confinement in the x -direction. In addition, due to the increased coupling of the density in a direction perpendicular to the wires, we pick up some weak Drude absorption at $\omega = 0$. The dashed curve labeled by the open square symbol tracks the location of this peak which follows closely the dispersion of the cyclotron mode $\omega = \omega_c$ up to the point where it interacts weakly with the 1DMP (open circles).

The peak positions as a function of B are shown in Fig. 6. As compared to Fig. 3, the anticrossing between the KM and the 1DMP has now been pushed down in magnetic field so that there is already a strong interaction at $B = 0$ T. As a result, the frequency of the lower mode indicated by open circles decreases monotonically for the entire range of magnetic fields presented, and at higher magnetic fields has the character of the 1D EMP. The mode indicated by open diamonds attains a noticeable signal at $B \approx 0.8$ T as it evolves into the KM. However, unlike the case of lower electron density, the oscillator strength of the KM is shared with higher lying modes indicated by the open triangles and stars in Fig. 6. Although the triangle mode in the figure is very weak, it appears more prominently in the FIR absorption spectrum when the radiation is polarized along the wires. This mode is the same $q_y = 2\pi/a$ mode discussed earlier (triangles in Fig. 3) but in this case it interacts with another mode near $B = 1.5$ T and continues along the starred branch at higher magnetic fields where its strength is comparable to that of the KM.

The agreement with the experimental data (filled squares) is again very good, except in the vicinity of the Bernstein mode at $2\omega_c$. Our model provides a smooth and continuous interpolation through this region. The lower experimental branch closely follows the 1DMP indicated by open circles while the upper branch is clearly associated with the KM (open diamonds).

The weak structure in the trajectory of the lower experimental branch seen near ω_c can be explained in terms of the pair of $q_y = 2\pi/a$ modes which appear to anticross in Fig. 4(c). In the present situation, these modes are excited by virtue of the $2\pi/a$ modulation along the wire length. To confirm our interpretation of this kink-like feature, we considered a further increase in the density of the system without changing the potential used to generate Fig. 1(c). The density profile associated with this situation is shown in Fig. 1(d). Figure 7 illustrates the FIR power absorption of the system, and Fig. 8 shows the peak positions as a function of the magnetic field. Comparing Fig. 8 with Fig. 4(c), we see that these dispersions share several common characteristics. In particular, we see that the open diamond and triangles in Fig. 8 have the same qualitative behaviour as the two $q_y = 2\pi/a$

modes starting at $\omega \simeq 45 \text{ cm}^{-1}$ in Fig. 4(c). Also, the strong anticrossing between the open circles and open squares in Fig. 8 clearly has the same origin as the anticrossing between the 1DMP and the EMP mode in Fig. 4(c). Thus, the weak “kink” in the experimental data of Ref. [5] is associated with the anticrossing of the $q_y = 2\pi/a$ 1DMP and EMP modes which are excited by the $G = 2\pi/a$ modulation along the wire direction. As Fig. 4 indicates, the apparent coupling between the 1DMP and EMP modes decreases as the magnitude of the uniaxial modulation increases. This explains why the “kink” feature is more apparent at higher densities and gets progressively weaker as the wires become increasingly isolated from each other.

III. CONCLUSIONS

In this paper, we have studied the magnetoplasmon excitations in an array of periodically modulated quantum wires within the TFDW approximation. We have shown that the modulation along the wire direction effectively acts as a grating coupler which induces a coupling between the $\mathbf{q} = 0$ Kohn mode and the $\mathbf{q} = (0, 2\pi/a)$ 1D plasmon, resulting in a resonant anticrossing of these modes at a finite magnetic field. We have compared our theoretical results with the data of Ref. [5], and found excellent agreement for all density and magnetic field regimes investigated. In addition, we have provided a simple explanation for the kink feature at $\omega = \omega_c$, which was observed, but not explained, in Ref. [5]. Based on the overall agreement between theory and experiment, we believe that the underlying ground state densities used in the calculations, as illustrated in Fig. 1, are in fact a realistic representation of the density profiles produced in the experiments.

ACKNOWLEDGMENTS

We would like to thank M. Hochgräfe, R. Krahne, and D. Heitmann for useful discussions and for providing access to their experimental data. This work was supported by a grant from the Natural Sciences and Engineering Research Council of Canada.

REFERENCES

- ¹ *Nanostructures and Mesoscopic Systems*, edited by Bernhard Kramer (Plenum, New York, 1991); J. H. Davies, *The Physics of Low-Dimensional Semiconductors: An Introduction* (Cambridge University Press, United Kingdom, 1997).
- ² U. Mackens, D. Heitmann, L. Prager, and J.P. Kotthaus, Phys. Rev. Lett. **35**, 1485 (1984)
- ³ *Electronic Properties of Multilayers and Low-Dimensional Semiconductor Structures*, edited by J. M. Chamberlain, L. Eaves, and J. C. Portal (Plenum, London, 1989)
- ⁴ D. Heitmann and J. P. Kotthaus, Phys. Today **46**, 56 (1993).
- ⁵ M. Hochgräfe, R. Krahne, Ch. Heyn, and D. Heitmann, Phys. Rev. B **60**, R13974 (1999).
- ⁶ G. Eliasson, Ji-Wei Wu, P. Hawrylak and J. J. Quinn, Solid State Commun. **60**, 41 (1986).
- ⁷ B. P. van Zyl and E. Zaremba, Phys. Rev. B **59**, 2079 (1999).
- ⁸ E. Zaremba and H.C. Tso, Phys. Rev. B **49**, 8147 (1994).
- ⁹ E. Zaremba, Phys. Rev. B **53**, R10512 (1996).
- ¹⁰ B. P. van Zyl and E. Zaremba, Phys. Rev. B **61**, 2107 (2000).
- ¹¹ B. P. van Zyl and E. Zaremba, Physica E **6**, 423 (2000).
- ¹² That is, the form of the equilibrium density is not chosen arbitrarily. Perturbations of the system away from the equilibrium state generate internal forces which drive the system back towards equilibrium. These forces are consistently included in the TFDW hydrodynamic equations used to describe the dynamics of the system. See, e.g., Ref. [7].
- ¹³ The choice for this confining potential is two-fold: (i) It allows us to *independently* vary the density coupling between adjacent wires by means of ω_0 and the degree of modulation along the wires by means of V_y and (ii) it appears to be the simplest potential that can still capture the most important features of the experimental data.
- ¹⁴ Details pertaining to the solution of Eqs. (3) and (4) can be found in Refs. [7,10].
- ¹⁵ The FIR power absorption data presented in Figs. 2, 5, and 7 have been generated with the phenomenological damping parameter $\gamma = 4.4 \text{ cm}^{-1}$. However, when peaks lie very close to each other, a smaller value of $\gamma = 2.2 \text{ cm}^{-1}$ allows us to better resolve the peak positions, especially for peaks having weak resonances.
- ¹⁶ J. F. Dobson, Phys. Rev. Lett. **73**, 2244 (1994), and references therein
- ¹⁷ T. Demel, D. Heitmann, P. Grambow, and K. Ploog, Phys. Rev. Lett. **66**, 2657 (1991).
- ¹⁸ H. Drexler, W. Hansen, J.P. Kotthaus, M. Holland, and S. Beaumont, Phys. Rev. B **46**, 12849 (1992).
- ¹⁹ V. Gudmundsson, A. Brataas, P. Grambow, B. Meurer, T. Kurth, and D. Heitmann, Phys. Rev. B **51**, 17744 (1995).
- ²⁰ A. L. Fetter, Ann. Phys. (N.Y.) **88**, 1 (1974).
- ²¹ D. E. Bangert, R. J. Stuart, R. E. Tyson and H. P. Hughes, Superlattices and Microstructures **13**, 225 (1993).

FIGURES

FIG. 1. Equilibrium density distributions, presented as surface and contour plots, for: (a) $\bar{n}_{2D} = 0.1$, $V_y = 1$ a.u., (b) $\bar{n}_{2D} = 0.2$, $V_y = 1$ a.u., (c) $\bar{n}_{2D} = 0.2$, $V_y = 2$ a.u., and (d) $\bar{n}_{2D} = 0.3$, $V_y = 2$ a.u. In all cases, $a = 600$ nm and $\omega_0 = 0.427$ a.u. The parameters pertaining to v_{ext} were chosen to reproduce the $B = 0$ T excitation frequencies in Ref. [5].

FIG. 2. Calculated FIR power absorption of the modulated quantum wire array corresponding to the density in Fig. 1(a). The unfilled symbols are used to label the various peak trajectories, denoted by the dashed lines. The incident radiation is polarized in a direction perpendicular to the wires.

FIG. 3. Theoretical B dispersion of the resonant FIR absorption data in Fig. 2. The unfilled symbols correspond to those in Fig. 2, and the filled squares are the experimental data from Ref. [5]. The dashed and full curves are explained in the text.

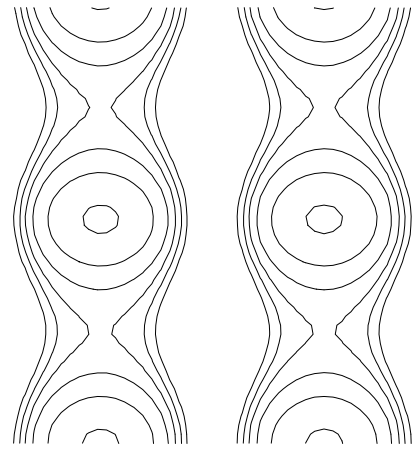
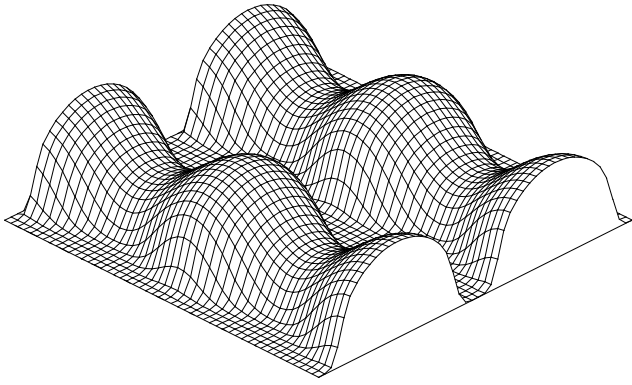
FIG. 4. Calculated B dispersions of the modes in a uniaxially modulated 2DEG at a fixed wavevector $\mathbf{q} = (0, 2\pi/a)$. The amplitudes of the modulating potentials are (a) $V_x = 0.25$ a.u. , (b) $V_x = 1.25$ a.u. , and (c) $V_x = 1.5$ a.u. The dashed line represents the cyclotron frequency.

FIG. 5. As in Fig. 2 but for an equilibrium density defined by Fig. 1(c).

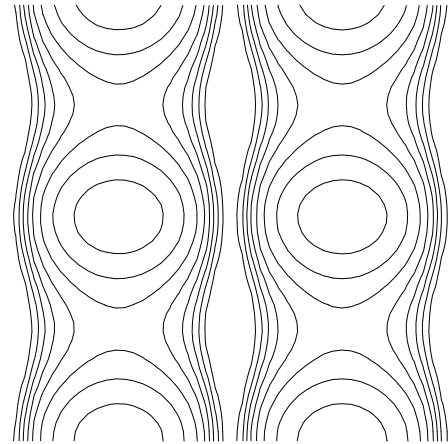
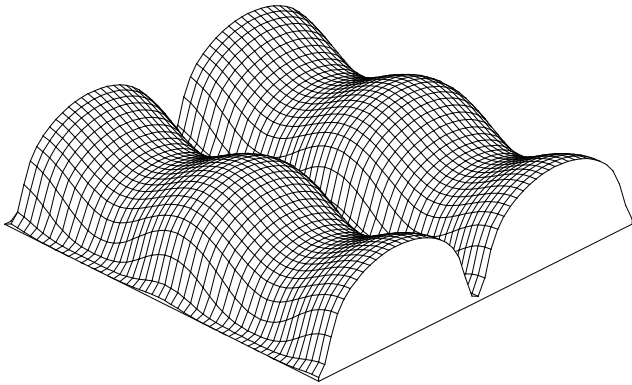
FIG. 6. As in Fig. 3, but with the data extracted from Fig. 5.

FIG. 7. As in Fig. 2, but for an equilibrium density defined by Fig. 1(d).

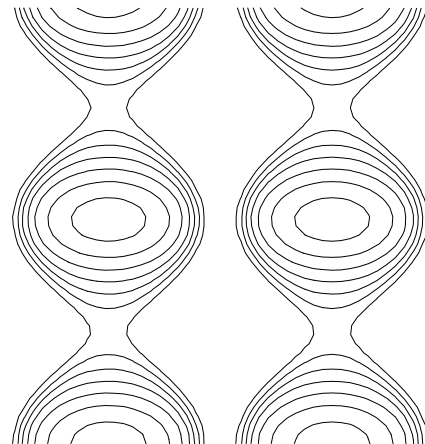
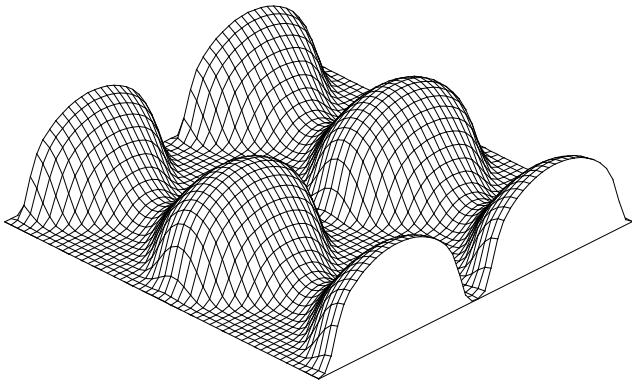
FIG. 8. As in Fig. 3, but with data extracted from Fig. 7.



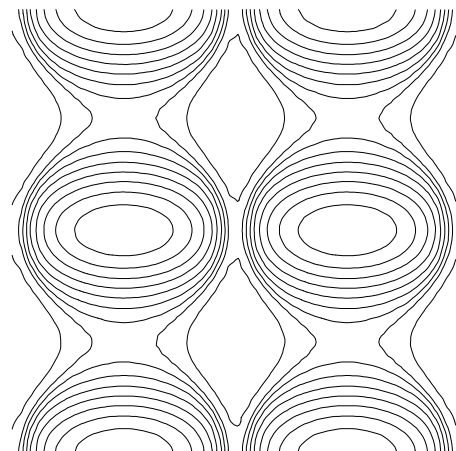
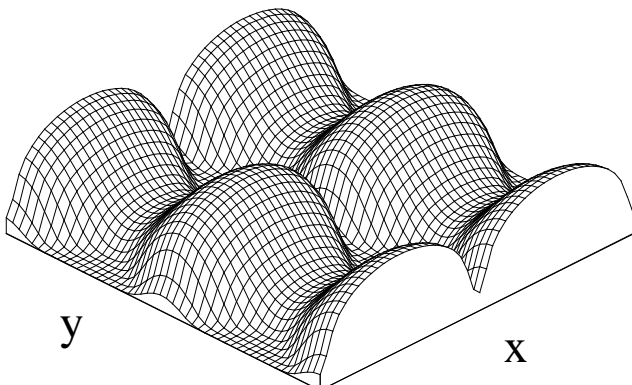
(a)



(b)



(c)

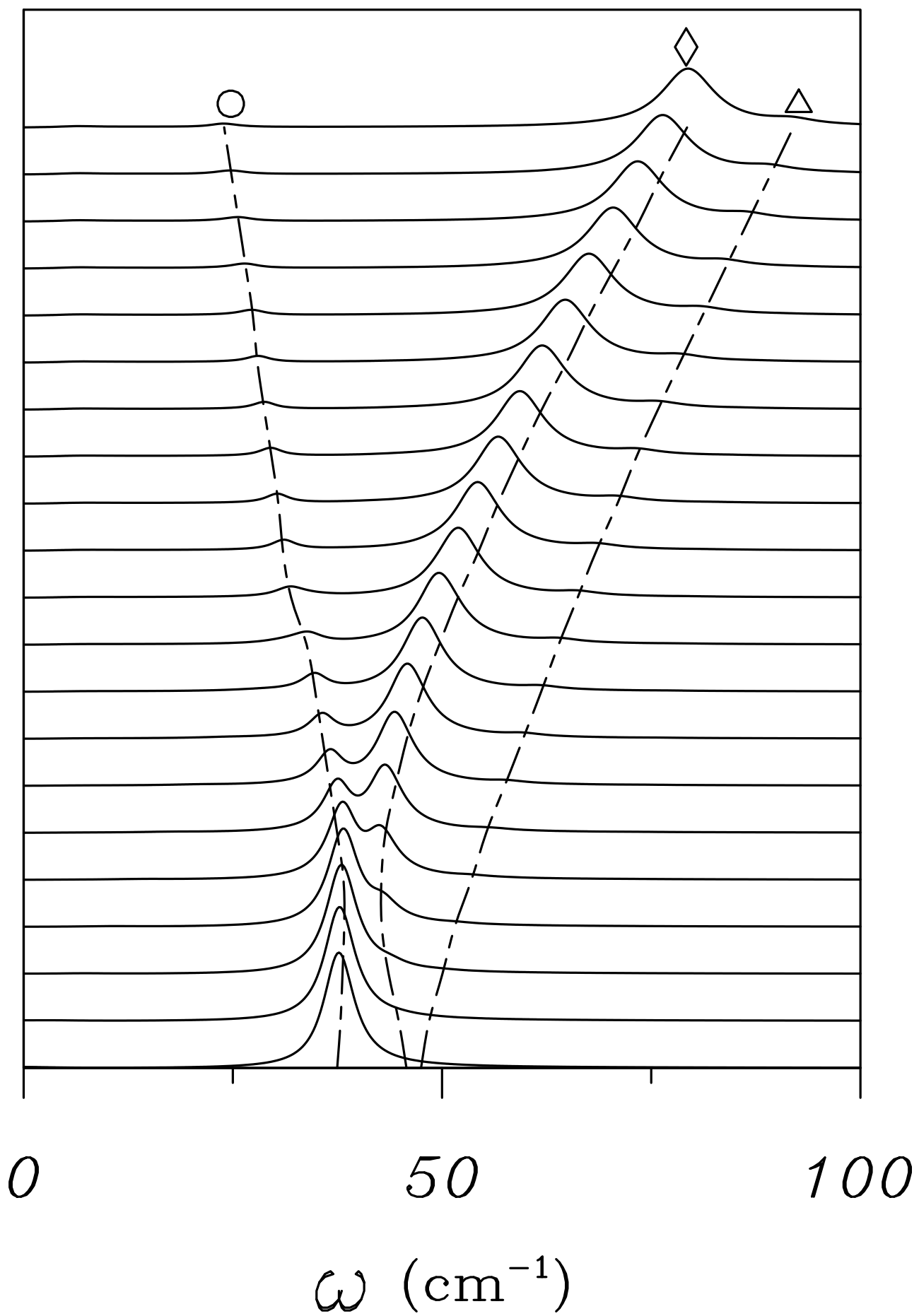


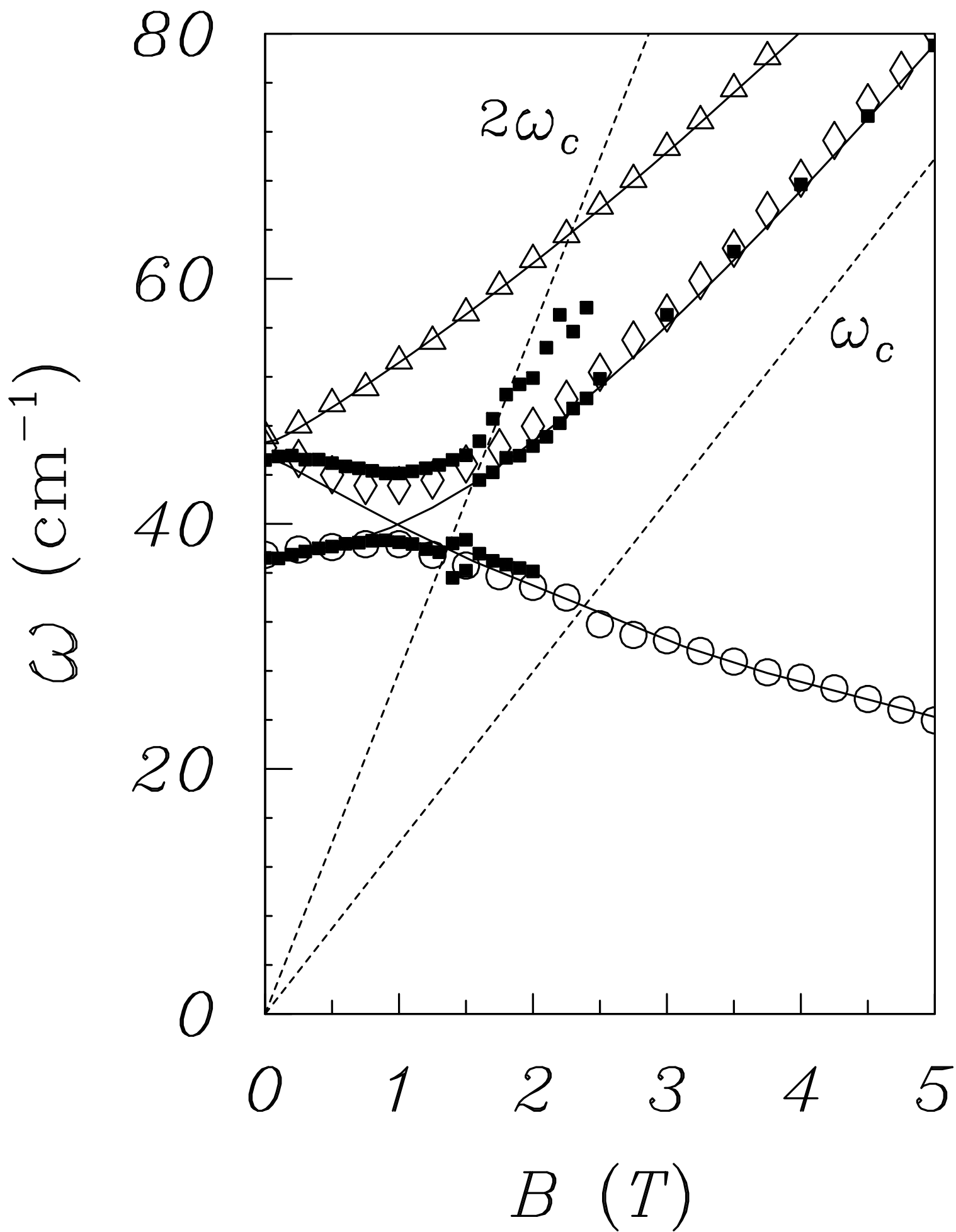
(d)

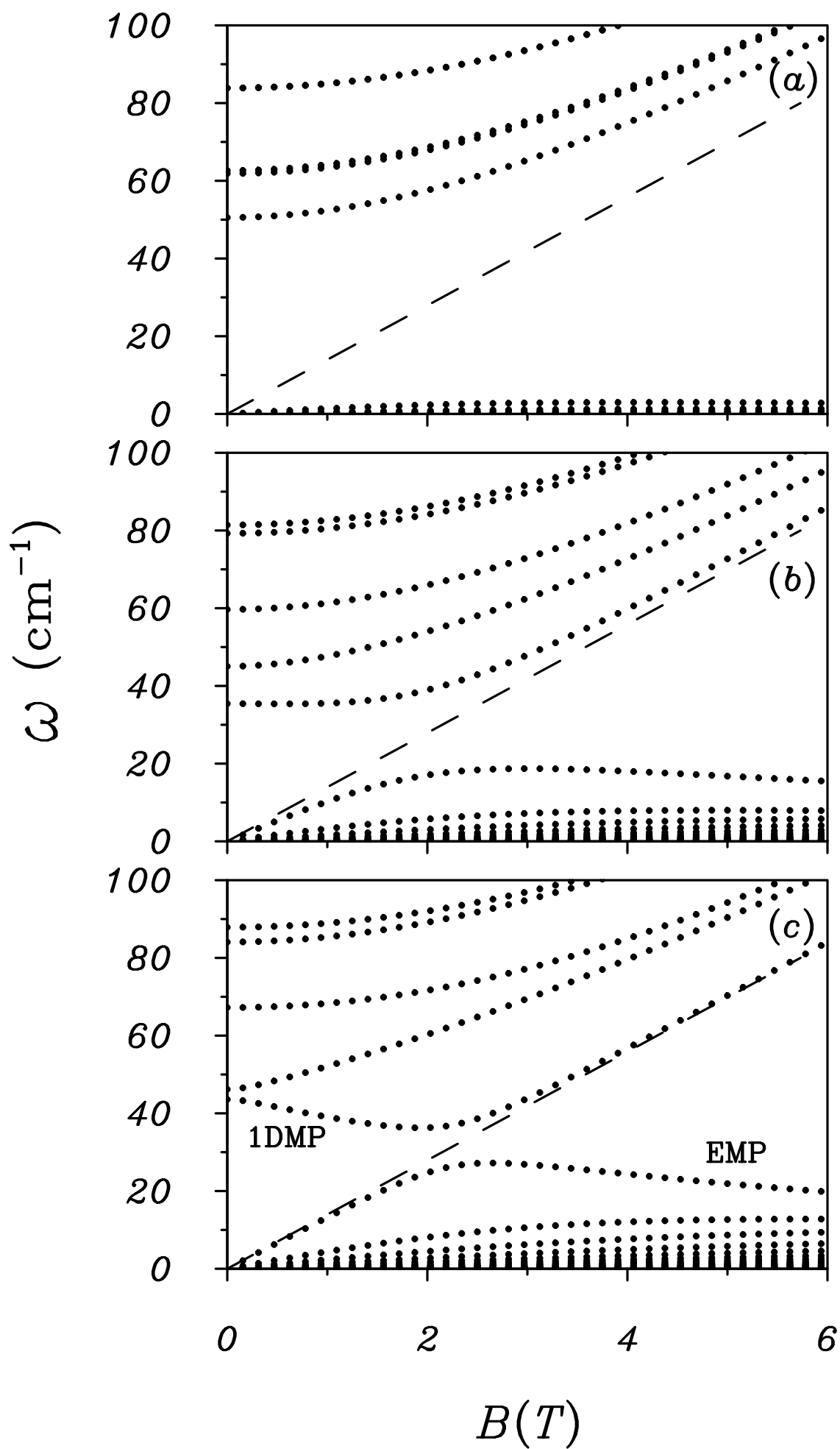
y

x

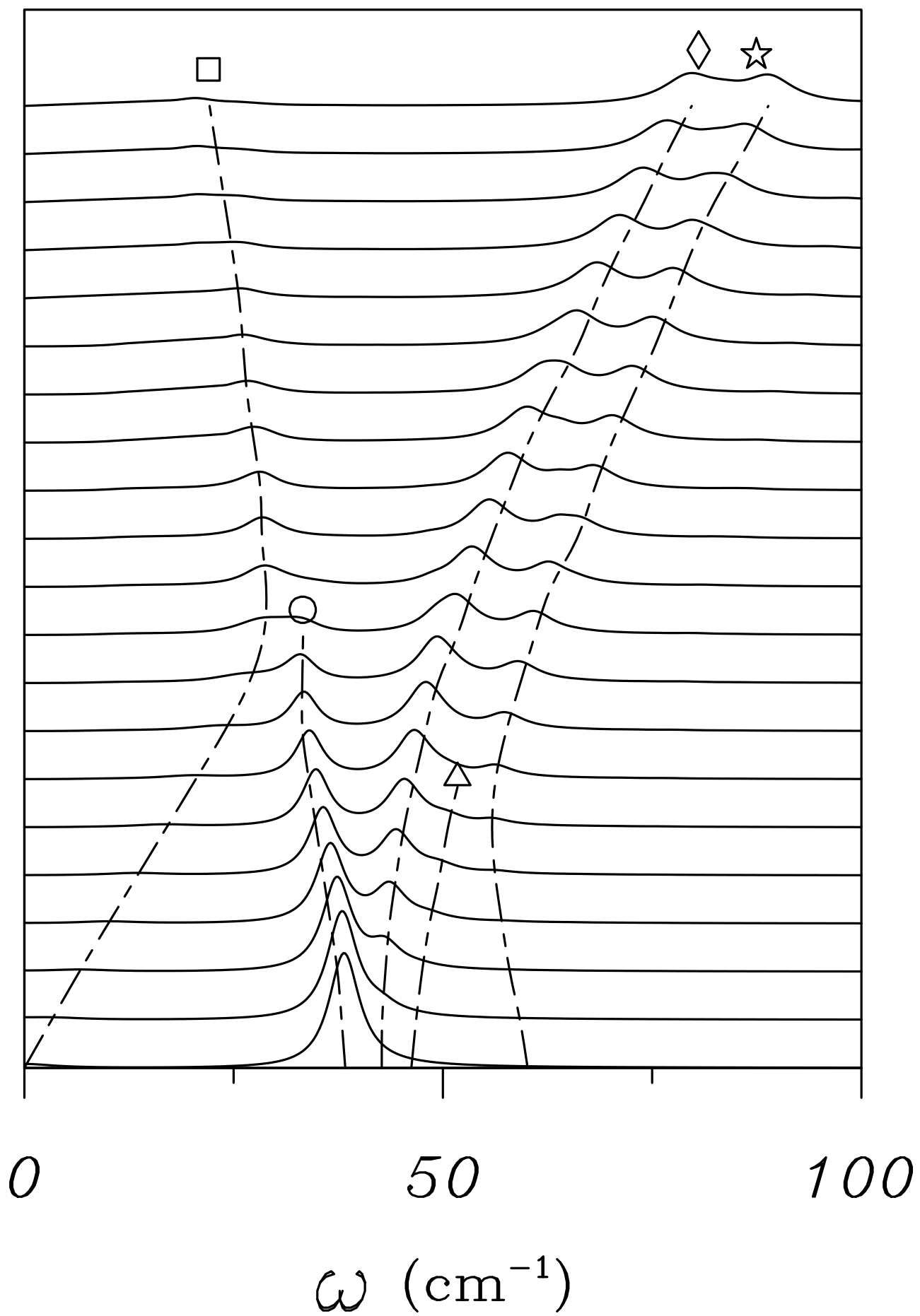
Power Absorption

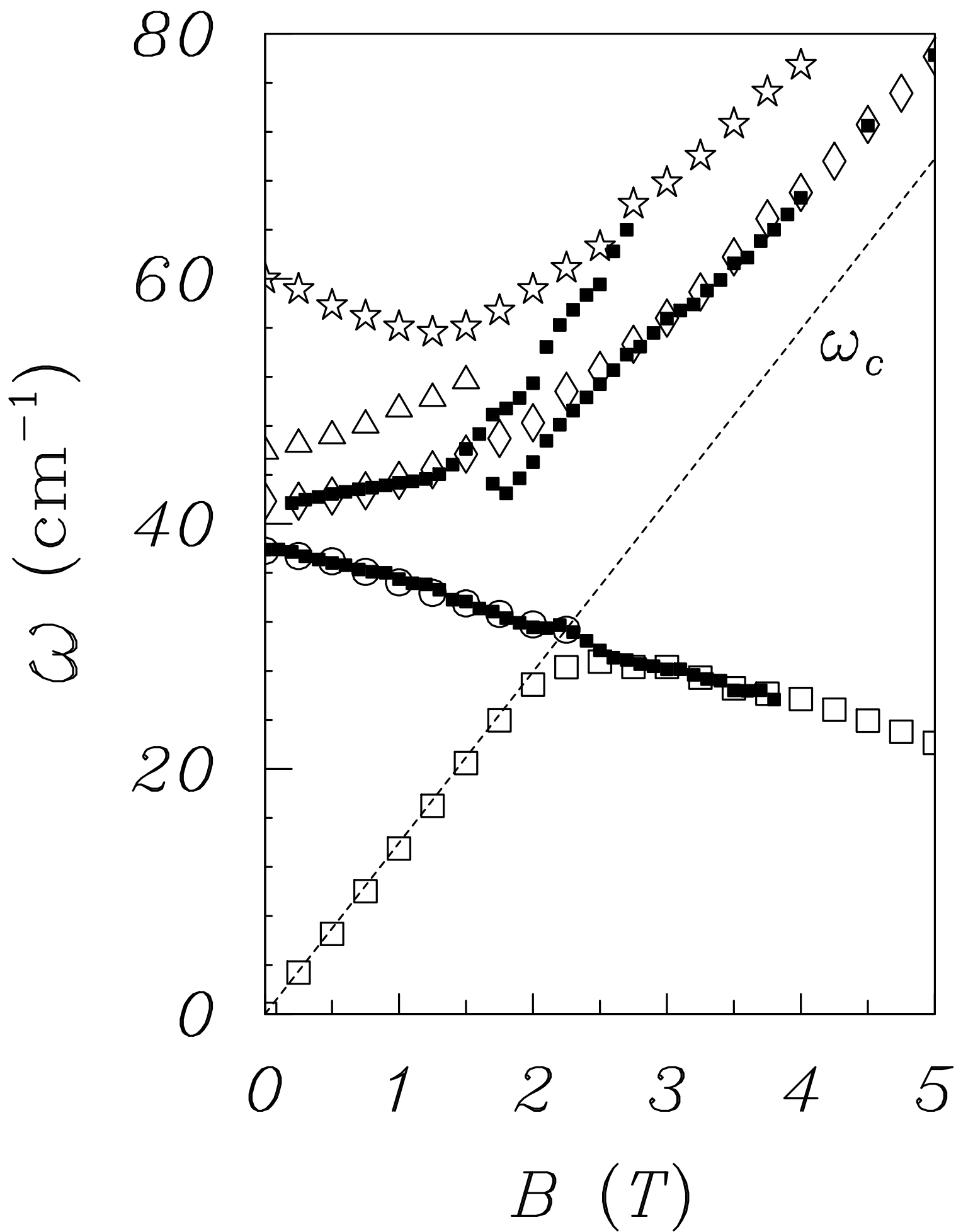






Power Absorption





Power Absorption

